

in a hydrothermally active oceanic crust.

The constancy of the  $\delta^{11}\text{B}$  value of uncontaminated OIBs ( $-9.9 \pm 1.3$  per mil) and its striking similarity with that of the bulk continental crust (21) suggests, in agreement with some current geochemical models, that crustal extraction took place from an initially homogeneous mantle source. It would imply that the primitive mantle had a rather constant  $\delta^{11}\text{B}$  value of  $\approx -10 \pm 2$  per mil. This should pose strong constraints on the type of chondrites from which Earth was formed and on the processes able to produce this homogenization during its accretion and differentiation, because of the variable  $\delta^{11}\text{B}$  values (29) found for chondritic materials.

## REFERENCES AND NOTES

1. The near-constant  $^3\text{He}/^4\text{He}$  ratio of MORBs worldwide ( $8 \pm 1 R_a$ , where  $R_a$  is the atmospheric value of  $1.386 \times 10^{-6}$ ) demonstrates that the source of MORBs, presumably the upper mantle, has been able to homogenize thoroughly  $^3\text{He}$ , which was trapped from the solar nebula during Earth's formation together with U and Th, which are the radioactive parents of  $^4\text{He}$ . In contrast,  $^3\text{He}/^4\text{He}$  ratios registered in OIBs vary widely from about  $5R_a$  up to  $30R_a$ , indicating mixing between a primitive He component enriched in  $^3\text{He}$  and various amounts of  $^4\text{He}$  generated from U-rich and Th-rich components such as subducted crust or sediments [J. E. Lupton, *Annu. Rev. Earth Planet. Sci.* **11**, 371 (1983)].
2. It has been recently proposed that  $^3\text{He}$  in the mantle may originate from recycling of sediments having incorporated meteoritic He [D. L. Anderson, *Science* **261**, 170 (1993)], because deep-sea sediments are known to contain interplanetary dust particles (IDPs) rich in solar He [M. Ozima, M. Takayanagi, S. Zashu, S. Amari, *Nature* **311**, 448 (1984)]. However, a recent diffusion experiment has shown that IDPs cannot retain He during subduction [H. Hiyagon, *Science* **263**, 1257 (1994)]. In addition, this hypothesis would require fluxes of meteoritic matter much higher than those having taken place during Earth's geological history [T. Trull, in *Noble Gas Geochemistry and Cosmochemistry*, J. Matsuda, Ed. (Terra Scientific, Tokyo, 1994), p. 77].
3. M. Chaussidon and A. Jambon, *Earth Planet. Sci. Lett.* **121**, 277 (1994).
4. M. Chaussidon and G. Libourel, *Geochim. Cosmochim. Acta* **57**, 5053 (1993).
5. At magmatic temperatures, isotopic fractionations of B are likely very small [M. R. Palmer, D. London, G. B. Morgan, H. A. Baab, *Chem. Geol.* **101**, 123 (1992)]. In addition, B being incompatible (4), this element is strongly partitioned in the melt, thus minimizing bulk isotopic fractionations due to melt-crystal equilibria.
6. Mantle melts always remain B-undersaturated because B exchanges primarily with Si in melts, even for high B contents of several percent by weight of  $\text{B}_2\text{O}_3$  [S. Chakraborty, D. B. Dingwell, M. Chaussidon, *Geochim. Cosmochim. Acta* **57**, 1741 (1993)]. In addition, B observed in volcanic fumaroles might largely be due to interactions between melts and seawater [M. Nomura, T. Kanzaki, T. Ozawa, M. Okamoto, H. Kakinana, *ibid.* **46**, 2403 (1982)].
7. A. J. Spivack and J. M. Edmond, *Geochim. Cosmochim. Acta* **51**, 1033 (1987).
8. A. J. Spivack, M. R. Palmer, J. M. Edmond, *ibid.*, p. 1939.
9. T. Ishikawa and E. Nakamura, *Nature* **370**, 205 (1994).
10. D. W. Graham, D. M. Christie, K. S. Harpp, J. E. Lupton, *Science* **262**, 2023 (1993).
11. B. Marty *et al.*, *Geochim. J.* **27**, 219 (1993).
12. B. Marty, unpublished data.
13. Analytical details are given in (3, 4). The B isotopic compositions are given as  $\delta^{11}\text{B}$  values (in per mil):  $\delta^{11}\text{B} = 1000 \times \{[(^{11}\text{B}/^{10}\text{B})_{\text{sample}} / (^{11}\text{B}/^{10}\text{B})_{\text{NBS 951}}] - 1\}$  with  $(^{11}\text{B}/^{10}\text{B})_{\text{NBS 951}} = 4.40558$  [after M. Palmer and J. Slack, *Contrib. Mineral. Petrol.* **103**, 434 (1989)].
14. T. K. Kyser, J. R. O'Neill, I. S. E. Carmichael, *Contrib. Mineral. Petrol.* **81**, 88 (1982).
15. Four samples from the east rift zone of Kilauea volcano and three samples of Loihi seamount were earlier analyzed by ion probe and yielded  $\delta^{11}\text{B}$  values ranging between  $-7.4$  and  $+0.6$  per mil (3).
16. T. Ishikawa and E. Nakamura, *Geochim. Cosmochim. Acta* **56**, 1633 (1992).
17. J. A. Barrat, B. M. Jahn, S. Fourcade, J. L. Joron, *ibid.* **57**, 2291 (1993).
18. Isotope fractionations of B have not yet been determined experimentally, but it is anticipated that water-rock interactions decrease the  $\delta^{11}\text{B}$  of the rock: B in tetrahedral coordination is preferentially incorporated in the solid, and tetrahedral B is  $^{11}\text{B}$ -depleted as compared to trihedral B [H. Kakinana, M. Kokata, S. Shoshei, M. Nomura, N. Okamoto, *Bull. Chem. Soc. Jpn.* **50**, 158 (1977)]. This effect was found for altered rhyolites in the Yellowstone hydrothermal system [M. R. Palmer and N. C. Sturchio, *Geochim. Cosmochim. Acta* **54**, 2811 (1990)].
19. The  $^3\text{He}/^4\text{He}$  ratios of the melt can decrease through a combination of degassing during fractionation and ascent to the surface, resulting in a loss of  $^3\text{He}$ -rich mantle He and in magma ageing, which results in a buildup of radiogenic  $^4\text{He}$  [D. E. Fisher and M. R. Perfit, *Nature* **343**, 450 (1990)]. It was also convincingly shown for the BABB glasses from the Lau basin and Valu Fa ridge that variations in the  $^3\text{He}/^4\text{He}$  ratios between  $2.4R_a$  and  $8.5R_a$  were due to local assimilation of old altered oceanic crust [D. R. Hilton, K. Hammerschmidt, G. Looock, H. Friedrichsen, *Geochim. Cosmochim. Acta* **57**, 2819 (1993)].
20. M. R. Palmer, *Geology* **19**, 215 (1991).
21. J. D. Morris, W. P. Leeman, F. Tera, *Nature* **344**, 31 (1990).
22. M. Chaussidon and F. Albarède, *Earth Planet. Sci. Lett.* **108**, 229 (1992).
23. A. Zindler and S. R. Hart, *Annu. Rev. Earth Planet. Sci.* **14**, 493 (1986).
24. C. Hémond, C. W. Devey, C. Chauvel, *Chem. Geol.* **115**, 7 (1994).
25. C. Chauvel, A. W. Hofmann, P. Vidal, *Earth Planet. Sci. Lett.* **110**, 99 (1992).
26. J. G. Ryan and C. H. Langmuir, *Geochim. Cosmochim. Acta* **57**, 1489 (1993).
27. This budget is calculated for a maximum mass of the depleted mantle of  $2.0 \times 10^{27}$  g as estimated from K, Rb, and Cs systematics (30), of  $0.13 \times 10^{25}$  g for seawater and of  $2.25 \times 10^{25}$  g for the continental crust. The B content of seawater is 4.5 ppm (7), and a mean of 10 ppm is assumed for the continental crust [H. Harder, in *Handbook of Geochemistry II*, K. H. Wedepole, Ed. (Springer-Verlag, Berlin, 1978), vol. 1, p. 5E5].
28. P. J. Michael and J. G. Schilling, *Geochim. Cosmochim. Acta* **53**, 3131 (1989).
29. Six chondritic meteorites, analyzed by the chemical extraction of B and mass spectrometry, have bulk  $\delta^{11}\text{B}$  values between  $-8.5$  and  $+1.8$  per mil [E. K. Ageyi and C. C. McMullen, *U.S. Geol. Surv. Open-File Rep.* 78-701 (1978), p. 3]. Ion probe analyses of the Orgueil meteorite gave a mean  $\delta^{11}\text{B}$  value of  $-2 \pm 5$  per mil [M. Chaussidon and F. Robert, *Nature* **374**, 337 (1995)], and they revealed very large small-scale variations (between  $\approx -50$  and  $\approx +40$  per mil) in single chondrules.
30. W. F. McDonough, S.-S. Sun, A. E. Ringwood, E. Jagoutz, A. W. Hofmann, *Geochim. Cosmochim. Acta* **56**, 1001 (1992).
31. Y. Sano and B. Marty, in preparation.
32. We thank K. Harpp, D. W. Graham, Y. Sano, and C. W. Devey for providing samples and making unpublished data available. We are indebted to C. France-Lanord for oxygen isotope measurements of Manus samples. This is Centre de Recherches Pétrographiques et Géochimiques-Centre National de la Recherche Scientifique contribution 1121.

14 February 1995; accepted 16 May 1995

## Late Miocene Tidal Deposits in the Amazonian Foreland Basin

Matti E. Räsänen,\* Ari M. Linna, José C. R. Santos, Francisco R. Negri

Late Miocene tidal sediments of Acre, Brazilian Amazonia, were deposited in an embayment or interior seaway located in the sub-Andean zone. This late Tertiary embayment system may once have connected the Caribbean with the South Atlantic. The tidal coasts of the embayment-seaway have provided an avenue for the earliest waif (over water) dispersal phases of the great American biotic interchange in the late Miocene. The subsequent change from semimarine to terrestrial environments is of value in assessing the importance of earlier hypotheses on the evolution of the western Amazonian landscape and gives insight into the formation of several observed biogeographic patterns, especially of aquatic biota.

The southwestern Amazonian lowland is currently 100 to 200 m above sea level. The late Tertiary history of the area has been uncertain; a key area is the state of Acre, Brazil (Fig. 1). Several origins have been suggested for the fine-grained sedimentary deposits cropping out at Acre. One hypoth-

esis is that these deposits formed in a catastrophic Pleistocene flood resulting from sudden draining of glacial Lake Titicaca (1). Another is that they represent deltaic deposition in an enormous Pleisto-Holocene lake (Lago Amazonas) (2). A third is that they represent Mio-Pliocene fluvial deposition in an alluvial fan draining the Andes (3). Generally, they have been considered as fluvial in origin (4, 5) and part of the Plio-Pleistocene Solimões Formation (6). It has not been clear how these deposits relate to late Tertiary deposits farther south.

M. E. Räsänen and A. M. Linna, Department of Geology, University of Turku, FIN-20500 Turku, Finland.  
J. C. R. Santos and F. R. Negri, Laboratório de Pesquisas Paleontológicas, Universidade Federal do Acre, Campus Universitário Km 4, Rio Branco, Acre, Brazil.

\*To whom correspondence should be addressed.

In 1927, von Ihering (7) proposed, on the basis of North Atlantic related foraminifers in the marine upper Miocene rocks of Rio de la Plata, Argentina, that a Cretaceous to Eocene seaway connected the Caribbean to the South Atlantic through the sub-Andean zone. Later, a younger late Tertiary connection was suggested in biogeographic studies (8, 9). Here we demonstrate that the fine-grained deposits in Acre were deposited by mesotidal rhythmic sedimentation in a sub-Andean estuarine environment in the late Miocene [Huayquerian, South American land mammal age (SALMA) (10, 11)] about 10 million to 8 million years ago (Ma) (12). Middle Miocene to Pliocene semimarine to marine embayments have now been geologically documented to extend into Andean foreland basins in Argentina, Paraguay (13), Bolivia (14), northern Peru, Colombia (15), and Venezuela (16). Recently, Hoon (15) has documented indications of middle to late Miocene tidal sedimentary deposits also in the intracratonic Amazonas basin (Fig. 1).

We studied the deposits of the Solimões Formation along the Acre and Purus rivers and the Rio Branco—Cruzeiro do Sul highway in a 250-km-long transect trending

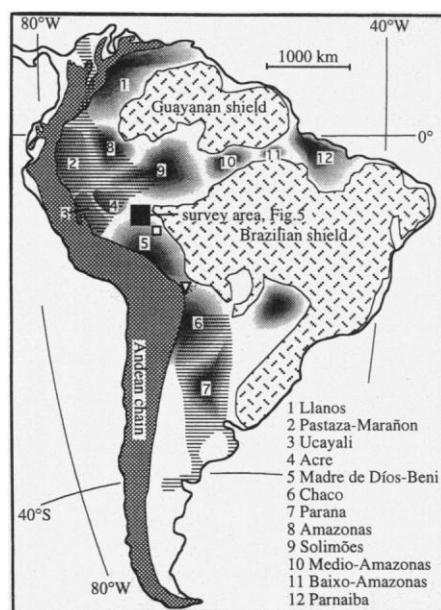


**Fig. 1.** Map showing the estimated limits of the northern middle to upper Miocene Pebasian and southern upper Miocene to Pliocene Paranaense marine to semimarine incursions (ruling) [after (9)]. The approximate location of Tertiary depocenters in the foreland (basins 1 through 7) and intracratonic (basins 8 through 12) sedimentary basins are depicted by shading. Light areas show the margins of the basins and the arches. Modified after (15, 32); ▽, area where the Yecua Formation has been documented; □, area where we have documented subtidal channel sediments with sand-mud couplets and inclined heterolithic stratification in the late Miocene Cobija Formation.

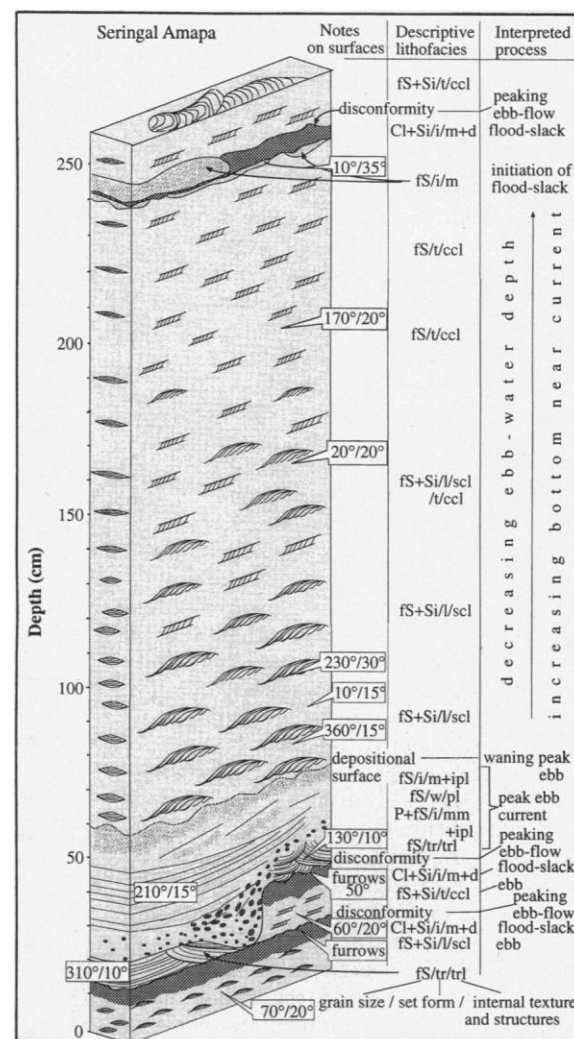
southeast to northwest across the non-flooded, generally flat, but dissected lowland terrain (*terra firme*) (Fig. 1). The surveyed area lies between the Acre, Solimões, and Madre de Dios—Beni basins on the continuation of the Fitzcarrald arch.

The sedimentary deposits along the transect form three distinct intercalated lithologic units. The channel lithosome (thickness, 2 to 10 m) is composed of rhythmically bedded, sand-mud couplets, and the mean thickness is 23.2 cm (range, 6 to 210 cm;  $n = 243$ ). The sand in the couplets is 5 to 200 cm thick and is composed of fine (mean diameter, 70 to 150  $\mu\text{m}$ ) lithic arenites, rich in plagioclase. The sand changes abruptly into mud. The mud layer is 1 to 15 cm thick and is regularly deformed and bioturbated. Thicker mud includes irregular

sand layers. Depending on the orientation of the section, the couplets either show inclined heterolithic stratification (IHS) (17, 18) tens or hundreds of meters in lateral extent or are trough-shaped (width, 10 to 100 m) with the couplets extending entirely along the basal unconformity (18). Higher in the section, the sand-mud couplets are thin and predominantly fine-grained. Channel lithosomes are often multilayered.

The internal structures of the sand-mud couplets (Fig. 2) and their architecture (Fig. 3A) show vertical subaqueous aggradation and successive lateral migration of the depositional surface of a point bar of a meandering channel (18). The frequent presence of IHS suggests that lateral channel migration was extensive. The trough-shaped channel lithosomes show

**Fig. 2.** Lithostratigraphy of a vertical section across four inclined sand-mud couplets in a channel lithosome 10 m thick with IHS (Fig. 3A). The lower parts of the two lowermost couplets (0 to 27 cm) exhibit ripple drift—cross lamination changing into a massive deformed graded layer of clay and silt. The upper surfaces of the muds in the couplets have furrows and represent a disconformity. The thick couplet (starting at 15 to 27 cm and extending to 240 cm), the most extensive one encountered in the area, is separated from the underlying couplet by an erosional disconformity in which the furrows are approximately parallel (about 50°) to the paleocurrents of the above ripples. The lowermost part (up to 60 cm) is composed of successive inclined plane beds, mud pebbles eroded from the mud layer of the underlying couplet, deposits of dunes (paleocurrent 130°), and slightly inclined plane beds, which turn into partly massive sand with intercalated inclined parallel lamination. A distinct wavy depositional surface succeeds the massive sand. The wavy form of the surface is due to scour pits of the first asymmetric ripples formed. The finest grains are concentrated in the ripple troughs and foresets. The following coset of asymmetric ripples (mainly northeastern paleocurrents, range 0° to 230°) grade into smaller asymmetric ripples with increasing stoss side erosion. Concurrently, the modal grain size of the sand becomes coarser starting at 70 to 100  $\mu\text{m}$  and extending to 100 to 150  $\mu\text{m}$ , and the content of fine grains (<50  $\mu\text{m}$ ) diminishes from 43 to 31%. The upper part (190 to 240 cm) of the ripple coset is therefore composed of coarser material than is the lower part (60 to 120 cm). Code for descriptive lithofacies: grain size: clay (C), silt (S), fine sand (fS), and mud pebbles (P); set form: tabular (t), lenticular (l), trough (tr), wedge-shaped (w), and irregular (i); internal texture and structures: massive (m), massive matrix supported (mm), parallel laminae (pl), inclined parallel laminae (ipl), sigmoidal cross laminae (scl), concave cross laminae (ccl), trough laminae (trl), deformation (d), and bioturbation (b). The direction and dip angles for the ripple foresets and inclined bedding are given.



upfilling of nonmigrating channels (18).

In the sand-mud couplets in Fig. 2, erosion of the furrows on the mud surface preceded deposition of sand. Bed load sedimentation was followed by the initiation of sedimentation from suspension (wavy depositional surface). In rippled sand, grain size coarsens upward and ripple migration increases, implying a change from deep-water sedimentation to sedimentation in decreasing water depth and a concurrent increase in the flow rate in shallower water. These trends are typical for the couplets in the study area.

Two alternative depositional environments for the channel lithosomes could be considered: fluvial or tidal. The sandy ripple cosets of the couplets are interpreted to have been deposited during a shallowing ebb tide because the sand coarsens upward and the sand-mud contact is abrupt. After a flood in a fluvial regime, the sand grain size would decrease during waning flow and the sand-mud contact would become gradual. The well-defined mud includes regular soft sediment deformation and occasional desiccation cracks, which implies that the sedimentation was cyclic, continuous, and rapid. The mud is interpreted to be deposited during flood tide, flood-slack in particular. The ripple-drift sands in the couplets generally exhibit consistent paleocurrent directions deviating about 90° from the dip direction of IHS (Fig. 5). This indicates that ebb flow was dominating in the tidal channels (19). Couplets with opposite-directed paleocurrents can be found locally in the basal parts of individual channels.

The upper half of the section in Fig. 3A shows a runoff channel. The channel is conformably covered by the next flood-mud layer and is interpreted as an ebb-runoff channel. It suggests intertidal origin and a mesotidal range (2 to 4 m) for this locality. Figure 3B shows the thickness variation of the sand-mud couplets along a laterally aggraded sedimentary unit. The periodicity indicates semidiurnal tidal deposition.

The Acrean channel lithosomes documented above are nearly identical in dimensions and structures to the ancient point-bar deposits of the late Cretaceous Middle McMurray Formation (20) and Horseshoe Canyon Formation (19) in North America. These are interpreted as having been formed in mesotidal influenced estuaries.

There is also a second type of sand-mud couplet in the channel lithosomes (Fig. 4). The ripple drift sands are similar to those in Fig. 2, but in the upper part of the couplet there is a mud doublet in which the muds are separated by structureless sand or deformed sand stringers. This couplet type, together with indications of paleocurrent in the sand in the doublet opposite the ebb ripples, indicates that the sand in the dou-

blet and the upper mud layer were deposited in a subtidal zone during flood tide. The upper flood-slack mud is thicker than the lower, less regularly preserved ebb-slack mud, showing a longer time for sedimentation of mud during flood tide and slack.

The channel lithosomes grade both laterally and vertically into interchannel lithosomes 2 to 3 m thick, as the ripple-drift sands in the couplets make room for mud in the thinning couplets. At the top of the section, thin sand laminations alternate with horizontal, thicker mud layers. Flame structures in the upper surface of the mud

horizons are regular. Bioturbation is frequent. The lithosome can also be structureless. Diagenetic gypsum crystals several centimeters long are abundant. This lithosome is interpreted as mud-flat deposit and is considered typical of mesotidal conditions (19).

The third lithosome type, bioturbated sand, is rarely exposed and seems to exceed 5 m in thickness. Rich in quartz and with poorly preserved, inclined parallel bedding, it may represent a severely bioturbated subaquatic sand. It was encountered at 93 and 111 km along the Trans-Amazonian Highway (Fig. 5).

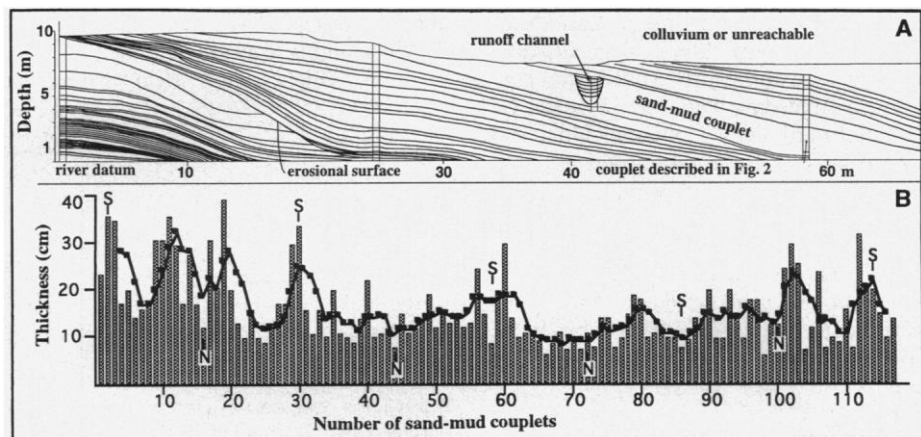


**Fig. 3.** (A) Cross-sectional profile (direction, 120° to 300°) of the IHS in a riverbank at Seringal Amapa close to Rio Branco (location given in Fig. 5). The sequence shows the sand-mud couplets (dip 15° in direction 90°) of a point bar, migrating laterally to the east. The section is perpendicular to the flow (20°), which has deposited the sand in the couplets. There is only one major erosive surface in the sequence. The 1.5-m-deep runoff channel in the sequence cuts sharply into the thickest sand-mud couplet. It is filled with a basal mud pebble conglomerate and massive sand, which pass upward into concave parallel lamination. It has knife-sharp noncollapsed erosional channel banks and is conformably covered by the next mud layer. Vertical columns show the detailed studied sections in the field. (B) Systematic thickness variation (bars) and their moving average (curve) of 117 sand-mud couplets along a laterally aggraded sedimentary unit comparable to (A) at Talisma (location given in Fig. 5). The moving average was calculated according to the thickness of four adjacent couplets. A semidiurnal 28-day periodicity was adapted; S, point of times for spring tides; N, point of times for neap tides.

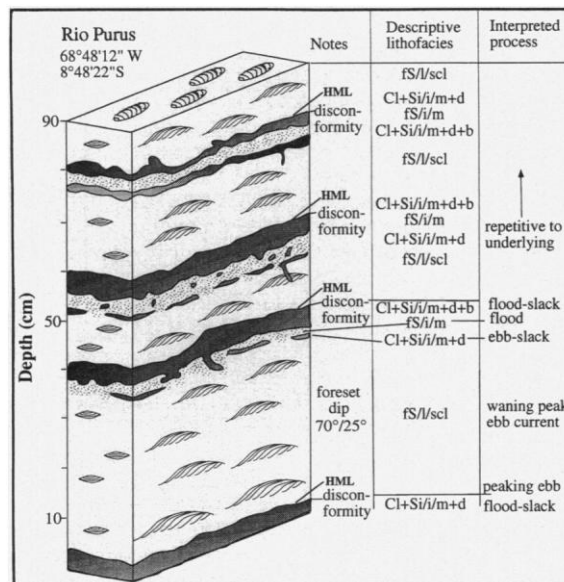


**Fig. 4.** Three complete sand-mud couplets with a mud doublet in their upper part. The sedimentation of every couplet initiated with the deposition of a heavy mineral layer (HML, mainly hematite and magnetite) on a disconformity during the first phase of suspension sedimentation of the waning flow. The paleocurrents of the ripples in all couplets are parallel to 70°. In the mud doublet, the lower, thinner, more deformed mud is followed by a massive sand with frequent mud pebbles. Location given in Fig. 5.

The three lithosomes described here indicate deposition in a coastal mesotidal environment. Paleocurrent measurements show northerly to southeasterly directions for the ebb flow (Fig. 5). The paleocurrent directions together with the mineralogy of the sediment indicate an Andean origin for the detritus.

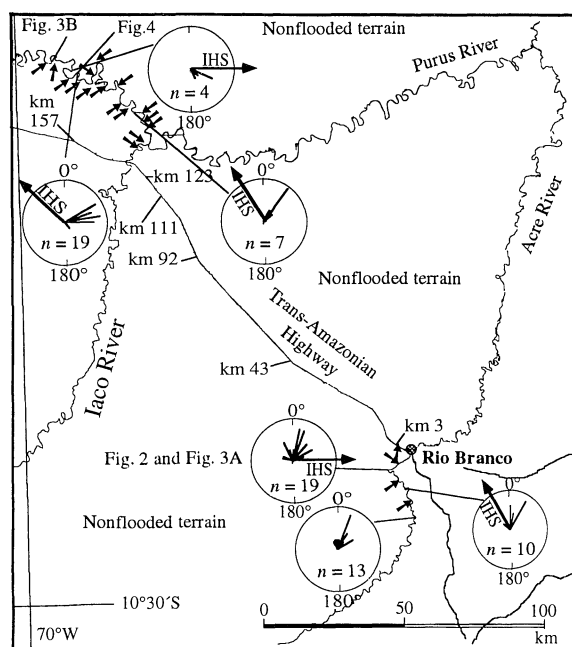
The absence of marine or semimarine mollusks shows that the water in this ebb-flow-dominated system may have had low salinity (19). However, the abundance of fossil fishes, turtles, and crocodilians (10, 11, 21) and some teeth of the euryhaline late-Miocene bullshark (*Carcharhinus*) in the sediments of Solimões Formation at the Acre River (22) indicate ample aquatic life and a marine connection. Marine fauna of sharks (Carcharinidae), stingrays (Myliobatidae), chimaeras (Chimaeridae), and cobs (Sciaenidae) have recently also been reported from the late Miocene Solimões Formation 500 km north of Acre (15). The fossil land-mammal fauna found at the locations (mainly in interchannel lithosomes) visited during this study along the Acre (23, 24) and Purus (24, 25) rivers, and the Rio Acre local fauna from the Solimões Formation (10, 26), are primarily correlated with the late Miocene Huayquerian SALMA. In Bolivia, the Huayquerian SALMA is dated around 10 to 8 Ma (12). Some faunal elements suggesting adjacent SALMAs exist, but these correlations seem not well validated.

Our results show that the late Miocene embayments or seaway reached the central part of South America (Fig. 1). This incursion concurs with the latest Serravallian high global sea stand ~10 Ma (27). We have recently observed tidal sediments dat-

ed as late Miocene (14) that crop out 200 km southwest of the Acre River, in the Madre de Dios-Beni basin in Bolivia (Fig. 1). We do not know if the above Acrean and northern Bolivian sedimentary deposits are part of the northern Pebasian inlet or if they derive from the southern Paranense marine incursion. The northernmost currently known deposits of Paranense incursion comprise the ~10-Ma-old Yecua Formation at depths of 3 km in the marginal zone of the Madre de Dios-Beni and Chaco basins (28) (Fig. 1). It is unclear whether the Pebasian and Paranense embayments were contemporary or were ever interconnected.

The extensive embayment-seaway environment surrounded by coastal tidal flats is analogous to the western interior seaway in North America that evolved during Cretaceous marine incursions. The coastal open habitats along the embayments served as a corridor between North and South America during the early waif dispersal phase of the great American biotic interchange (GABI) in the late Miocene (29). After the retreat of the embayments during the Plio-Pleistocene, huge areas in South America turned into aggrading alluvial plains. These seasonally flooded plains may have supported the migration of the North American savanna fauna through Amazonia during the later phases of GABI (30). The supposed savanna corridor promoting the migration may thus be not just climatically guided, as has been proposed earlier (31). In addition, the long-term landscape turnover from semimarine to terrestrial conditions has great potential to explain several observed sub-Andean biogeographic patterns, especially of aquatic biota (2, 8).

**Fig. 5.** Location of the field data at Acre. The paleo ebb-current directions from ripple-drift cross laminations of the tidal couplets are shown in the circles. IHS dip in the measured sections is also given. Small arrows show locations along the rivers where the channel lithosomes are well exposed. Sections along the Trans-Amazonian Highway are noted by their respective kilometer values. Channel lithosomes are at 3, 43, 123, and 157 km; interchannel lithosome is at 92 km. Along the highway the deposits are strongly weathered.



## REFERENCES AND NOTES

1. K. E. Campbell Jr. and C. D. Frailey, *Quat. Res.* **21**, 369 (1984); ———, L. Arellano, *Contrib. Sci.* **364**, 1 (1986).
2. C. D. Frailey, E. L. Lavina, A. Rancy, J. P. de Souza Filho, *Acta Amazonica* **18** (nos. 3–4), 119 (1988); B. I. Kronberg, R. E. Benchimol, M. I. Bird, *Interciencia* **16** (no. 3), 138 (1991).
3. E. Latrubesse, thesis, Universidad Nacional San Luis, Argentina (1992).
4. G. Klammer, in *The Amazon*, H. Sioli, Ed. (Junk, Dordrecht, Netherlands, 1984), pp. 47–83.
5. M. E. Räsänen, J. S. Salo, R. J. Kalliola, *Science* **238**, 1398 (1987); M. E. Räsänen, R. Neller, J. S. Salo, H. Junger, *Geol. Mag.* **129** (no. 3), 293 (1992).
6. *Levantamento de recursos naturais* (Ministério das Minas e Energia, Departamento Nacional da Produção Mineral, Projeto RADAMBRASIL, Rio de Janeiro, 1976), vol. 12.
7. H. von Ihering, *Die Geschichte des Atlantischen Ozeans* (Fischer, Jena, Germany, 1927).
8. E. Boltovskoy, *Lethaia* **24**, 191 (1991); H. H. Camacho, *Rev. Asoc. Geol. Argent.* **24** (no. 4), 357 (1969).
9. C. P. Nuttal, *Bull. Br. Mus. Nat. History Geol.* **45** (no. 2), 165 (1990); H. H. Camacho, *Rev. Asoc. Geol. Argent.* **22** (no. 4), 253 (1967).
10. C. D. Frailey, *Contrib. Sci.* **374**, 1 (1986).
11. C. Paula Couto, in *Anais do XXVIII Congresso Brasileiro de Geologia, Porto Alegre, Rio Grande do Sul, 27 Oct.–2 Nov.* (Sociedade Brasileira de Geologia, São Paulo, Brazil, 1976), pp. 237–249; *Iheringia Sér. Geol.* **5**, 3 (1978).
12. L. G. Marshall and T. Sempere, in *The Biotic Relationships Between Africa and South America*, P. Goldblatt, Ed. (Yale Univ. Press, New Haven, CT, 1993), pp. 329–392.
13. Late Miocene Anta Formation [A. Russo and A. Serraiotto, in *VII Congreso Geológico Argentino* (Asociación Geológica Argentina, Buenos Aires, Argentina, 1979), vol. 1, p. 715]; late Miocene-Pliocene Parana and Entre Rios formations [A. Russo, R. Ferello, G. Chebli, in *Segundo Simposio de Geología Regional Argentina* (Academia Nacional de Ciencias, Córdoba, Argentina, 1979), vol. 1, pp. 139–183].
14. Late Miocene Yecua Formation (~10 Ma) [L. G. Marshall and T. Sempere, in *Fosiles y facies de Bolivia*, Tomo 1: *Vertebrados*, R. Suarez-Soruco, Ed.; *Rev. Téc. Yacimientos Petrolíferos Fiscales Bol.* **12**, 631 (1991)].
15. Middle to late Miocene deposits of the Pebas Formation and the "Terciario Amazonico" [C. Hoorn, *Palaeogeogr. Palaeoclimatol. Palaeoecol.* **105**, 267 (1993); thesis, University of Amsterdam (1994)].
16. M. A. Lorente, *Diss. Bot.* **14**, 222 (1986).
17. R. G. Thomas et al., *Sediment. Geol.* **53**, 123 (1987).
18. W. Muwais and D. G. Smith, *Bull. Can. Pet. Geol.* **38**, 53 (1990).
19. D. G. Smith, in *Recent Developments of Fluvial Sedimentology*, F. G. Ethridge, R. M. Flores, M. D. Harvey, Eds. (Special Publication 39, Society of Economic Paleontologists and Mineralogists, Tulsa, OK, 1987), pp. 83–91.
20. G. D. Mossop and P. D. Flach, *Sedimentology* **30**, 493 (1983); D. G. Smith, *Bull. Can. Pet. Geol.* **36**, 216 (1988).
21. K. E. Campbell and C. D. Frailey, *Natl. Geogr. Soc. Res. Rep. 1977 Projects* (1985), p. 189.
22. A. Rancy, thesis, University of Florida (1991).
23. Edentata: Mylodontidae: *Urumacotherium*, *Ranculcus*; Rodentia: Hydrochoeridae: *Kiyutherium*; Dinomyidae: *Telcomys*, *Tetracyllus*, *Potomarchus*, *Phoberomys*; Neoeplimidae: *Neoeplima*; Notoungulata: Toxodontidae: *Trigodon*.
24. J. C. R. Santos, F. R. Negri, E. G. Silva, paper presented at XIII Congresso Brasileiro de Paleontologia—I Simpósio Paleontológico do Cone Sul, São Leopoldo, Rio Grande do Sul, Brasil, 19 to 26 September 1993.
25. Edentata: Orophodontidae: *Octodontobracys*; Mylodontidae: *Pseudoprepotherium*; Megalonychidae: cf. *Hapalops*; Rodentia: Dinomyidae: *Potamarchus*; Neoeplimidae: *Neoeplima*.
26. Faunal list of the Rio Acre local fauna [after (10)]: Chondrichthyes: Batoidea: Potamotrygonidae; Os-

- teichthytes: Osteoglossidae, Doradidae, Pimelodidae; Characidae: *Colossoma*; Callichthyidae; Reptilia: Chelonia: Pelomedusidae, Testudinidae; Crocodylia: Caviidae, Alligatoridae; Aves, Mammalia, Marsupialia, Edentata: Mylodontidae: *Stenodon campbelli*; Megalonychidae; Dasypodidae: Pamphathiinae; Rodentia: Erethizontidae; Dinomyidae: *Potomarchus murinus*, *Telcomys amazonensis*, *Tetrasylus*; Hydrochoeridae: *Kiyutherium orientalis*; Caviidae: Cardiomyinae, Neopibemidae, Dasypodidae; Echimyidae: Heteropsomyinae; Litopterna: Protheriidae, Macrauchenidae; Notoungulata, Astratheria, Sirenia: Trichechidae.
27. B. U. Haq, J. Hardenbol, P. R. Vail, *Science* **235**, 1156 (1987).
28. T. L. Gubels, B. L. Isacks, E. Farrar, *Geology* **21**, 695 (1993).
29. S. D. Webb, *Paleobiology* **2**, 216 (1976).
30. ———, *ibid.* **17**, 266 (1991).

31. ———, *Annu. Rev. Ecol. Syst.* **9**, 393 (1978); L. G. Marshall, *Am. Sci.* **76**, 380 (1988).
32. *Tectonic Map of South America, 1:5,000,000* (Departamento Nacional da Produção Mineral, Commission for the Geological Map of the World, UNESCO, Brasília, 1978).
33. We thank R. Dalrymple, P. Gibbard, S. Kroonenberg, J. Salo, D. G. Smith, and three anonymous referees for comments. Work in Brazil was supported by R. O. Kowmann and F. M. B. Cunha and the Universidade Federal do Acre; work in Bolivia by the Instituto Geológico de Bolivia, Yacimientos Petrolíferos Fiscales Bolivianos, and personally in the field by V. R. Lange, J. P. de Souza Filho, and J. B. Villanueva. The investigations were financed by the Academy of Finland (grants 1071377 and 1071443) and the Turku University Foundation.

22 November 1994; accepted 17 April 1995

## Female Responses to Ancestral Advertisement Calls in Túngara Frogs

Michael J. Ryan and A. Stanley Rand

Phylogenetic techniques were used to estimate and reconstruct advertisement calls at ancestral nodes. These calls were used to investigate the degree of preference of female túngara frogs (*Physalaemus pustulosus*) for both extant and ancestral calls. Females did not discriminate between calls of males of their own species and calls at their most recent ancestral node. They also recognized calls of three extant species and at four ancestral nodes as the signals of appropriate mates. Both shared ancestral history, and call convergence might differentially influence call preferences.

Differences in mate recognition systems behaviorally isolate species and are thought to be one of the most important causes of speciation; mate recognition, however, requires coordination of signal and receiver (1). The fact that such coordination characterizes many species is evidence that this functional association persists, but it tells us little of the historical patterns by which it arose. Species-specific mate recognition could evolve by the coordinated divergence of signal-receiver interactions of each incipient species, as has been suggested by some hybridization studies (2). Alternatively, the evolution of signals and receivers could occur in a more haphazard manner, in which stimuli that make signals more or less preferred are gained or lost through evolutionary history. In this case, other aspects of the calls that are perhaps irrelevant to the receiver preference could result from stochastic processes, constraints, or selection in other contexts, as has been argued from studies showing asymmetric mating preferences among species (3).

To truly understand how species recognition evolves, it is preferable to investigate directly the signals and receivers of ances-

tral species. The unique geological history of the Hawaiian islands and the amazing diversity of its indigenous fruit flies have

allowed such an approach to studies of mate recognition (3). In most studies, however, there are no clear ancestor-descendent relations among extant species. We have partially circumvented this problem by estimating and reconstructing the mate recognition signals at ancestral nodes; these nodes represent hypothesized ancestral species. We then conducted phonotaxis experiments to quantify female responsiveness to these signals. These experiments determined if the female's response was elicited only by the conspecific call, as would be suggested by the coordinated divergence of signal and receiver, or if ancestral calls contained key stimuli that effectively elicited a response, as is concluded from studies of mating asymmetries. If females were responsive to heterospecific calls, including those of both extant and hypothesized ancestral species, we also determined the degree to which female preferences were influenced by phylogenetic divergence and overall call similarity.

We examined the advertisement calls and phylogenetic relations of five species of frogs in the *Physalaemus pustulosus* species group and three of their close relatives (Fig. 1). The túngara frog, *P. pustulosus*, is sympatric with *P. enesefae* in Venezuela and allopatric with the other species. For 10 individuals of each species, 12 call parameters were measured and average calls were digitally synthesized with these variables (4) (Fig. 1). Phylogenetic relations were determined from an analysis of several morpho-

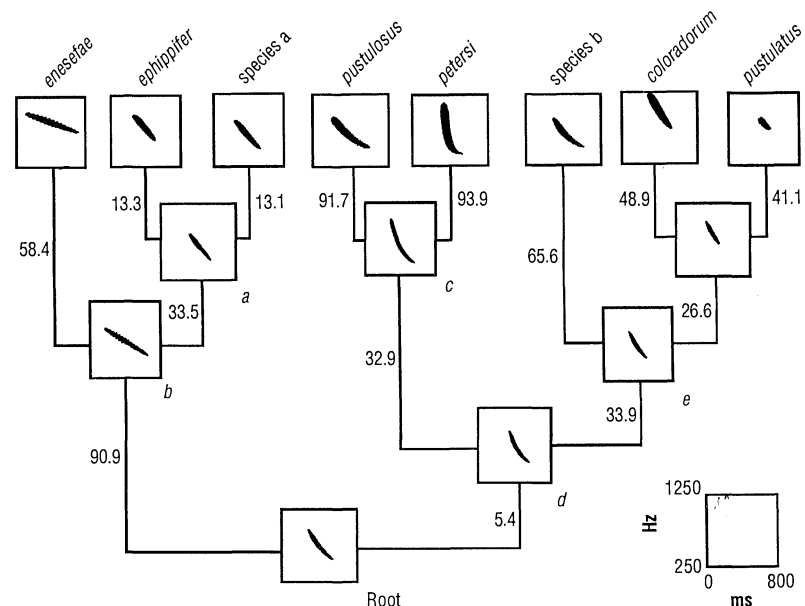


**Fig. 1.** The phylogenetic relations of frogs of the *P. pustulosus* species group and three closely related species (*P. enesefae*, species a, and *P. ephippifer*) (5). Species a and species b are undescribed. Shown are sonograms of the synthetic advertisement calls, which were determined from species' means for the extant (tip) species (4) or from phylogenetic estimates for calls at the ancestral nodes (7). Branch lengths are estimates of changes in mitochondrial DNA base sequences (7). A discriminant function analysis shows that 92% of the individuals of extant species, 10 per species, are assigned to the correct species by call alone. Numbers indicate branch lengths (7).

M. J. Ryan, Department of Zoology, University of Texas, Austin, TX 78712, USA, and Smithsonian Tropical Research Institute, Apdo. 2072, Balboa, Panama.  
A. S. Rand, Smithsonian Tropical Research Institute, Apdo. 2072, Balboa, Panama.